Measurements of double- and triple-spin parameters in *pp* elastic scattering between 440 and 560 MeV

E. Aprile,* R. Hausammann, E. Heer, R. Hess, C. Lechanoine-Leluc, W. R. Leo,†
S. Morenzoni, Y. Onel, D. Rapin, and P. Y. Rascher
Département de Physique Nucléaire et Corpusculaire, Université de Genève, 1211 Geneva 4, Switzerland

S. Jaccard, J. A. Konter, and S. Mango
Schweizerisches Institut fur Nuklearforschung, 5234 Villigen, Switzerland
(Received 19 May 1986)

The polarization parameter P_{n000}, the two-spin parameters D_{n0n0}, K_{n00n}, D_{s0s0}, D_{s0k0}, and the three-spin parameters M_{s0sn} and M_{s0kn} have been measured for *pp* elastic scattering between 34° and 118° center-of-mass scattering angle at six different incident kinetic energies 447, 473, 497, 517, 539, and 560 MeV. The experiment was performed at SIN using a polarized proton beam, a polarized butanol target, and a polarimeter for the measurement of the polarization of the scattered proton.

I. INTRODUCTION

The aim of this experiment was to obtain information on the *pp* elastic-scattering amplitudes in the angular range 34°—118° c.m. at energies between 400 and 579 MeV. Interest in this energy domain has been generated by the observation of energy-dependent structures first in $\Delta\sigma_L$ measurements in elastic *pp* scattering,[1] and then in the it_{11} (Ref. 2) and t_{20} parameters[3] in πd scattering. The existence of dibaryon resonances has been proposed to explain these phenomena. But in other experiments, the observed structure in t_{20} has not been observed,[4–6] and progress in *N-N* theory (e.g., Ref. 7) seems now to suggest that dibaryon resonances are not needed. Nevertheless phase-shift analyses of *N-N* elastic scattering,[8–11] agree on the existence of anticlockwise loops in the Argand diagrams for the $^1D_2$ (with mass around 2.14 GeV) $^3F_3$ and $^1G_4$ partial waves, although the behavior for the latter two must still be confirmed. Whether these half loops are due to inelastic thresholds as proposed for instance by Kloet *et al.*[12] or resonances, is still not clear. The Saclay data,[13] mainly at energies above 800 MeV, should help clarify the situation. But to have a complete understanding, a study of the inelastic channels $pp \rightarrow \pi^+ d, pn\pi^+, pp\pi^0$ is also essential. A rather large experimental effort is being put into this at present.

A purely experimental solution to the elastic *N-N* problem, however, also exists in the so-called "complete" experiment,[14] the measurement of a sufficient number of observables concerning the reaction at a given energy and angle, such as, to allow a complete reconstruction of the amplitudes directly from the data. For *pp* elastic scattering, this requires the measurement of about 12 or more well-chosen observables (differential cross section, and e.g., polarization, spin correlations, etc.) out of a possible 25 at each given angle and energy—a relatively large task. The results, however, would provide unambiguous and completely model-independent information on the scattering amplitudes. They would also provide a rigorous test of current and future theories of the *N-N* interaction as well as providing fixed anchor points for many of the phenomenological models currently in use. This was the aim of our elastic *pp* scattering experimental program at SIN.

This program began with measurements of the spin-correlation parameters A_{00nn} (Ref. 15) at seven energies between 350 and 580 MeV and measurements of A_{00ss}, A_{00kk}, and A_{00ks} (Ref. 16) at five energies. These data were then completed with measurements involving rescattering on a carbon polarimeter to observe the transverse polarization of the scattered proton, i.e., D_{n0n0}, K_{n00n}, D_{s0s0}, D_{s0k0}, M_{s0sn}, and M_{s0kn}. The data at 579 MeV have been published,[17,18] as well as the associated direct amplitude reconstruction in Refs. 18 and 19, the former one containing the c.m. angular region reconstruction between 38° and 58°. From these data also, a time-reversal-violating amplitude analysis[20] was done which sets an upper limit for time-reversal invariance in the strong interaction. Results on some spin-dependent parameters below 400 MeV will also soon be available.

In this paper we will present measurements of double- and triple-spin parameters at 447, 473, 497, 517, 539, and 560 MeV. Only at four of these energies, namely, 447, 497, 517, and 539 MeV, have enough parameters been measured to do an amplitude reconstruction. This analysis is in progress and will be discussed in a separate paper which will be available soon. Since the experimental setup and analysis are identical to the one presented in detail in Ref. 17, this article will concentrate mainly on those points relevant to these particular data. Our results will be compared to other existing measurements, as well as with phase-shift-analysis predictions. Typical statistical errors on these data were $\approx \pm(0.01\text{—}0.02)$ for P_{n000}, $\pm(0.01\text{—}0.04)$ for K_{n00n}, $\pm(0.02\text{—}0.06)$ for the *D*, and $\pm(0.03\text{—}0.08)$ for the *M* parameters.

II. EXPERIMENTAL SETUP

A complete description of the experimental setup can be found in Refs. 17 and 21. Two types of polarized beams were used for these experiments: (1) a "scattered" beam which was obtained by scattering the main SIN un-

polarized beam at 8° from an 8-mm-thick Be target (polarization $P_b = 0.4165 \pm 0.0043$) and (2) an "accelerated" beam in which polarized protons were produced directly by the atomic source and then accelerated to 580 MeV ($P_b = 0.8$ typically). In both cases change of direction of the spin vector was performed by a combination of two superconducting solenoids sandwiching the last deflecting magnet. Moreover, for the "accelerated" beam a fast periodic spin flip was performed directly at the ion source allowing a better control of systematic errors.

A schematic diagram of the detector layout is shown in Fig. 1. The polarized proton beam was scattered from a polarized target (PPT), cylindrical in shape, 2 cm in height and 2 cm in diameter. The target sample, which was composed of butanol droplets immersed in liquid ^{3}He at 0.5 K temperature, was placed in a 25-kG vertical magnet field created by two superconducting coils. The geometry was such that easy access to a wide angular range was possible. Typical target polarizations P_t were about 40–60%. A dummy target consisting of a copper cylinder of the same size, filled with carbon grains was suspended below the butanol target for background measurements.

Scattered and recoil particles were detected by two X-Y telescopes each consisting of three multiwire proportional chambers and a scintillation counter. The spin of the final-state proton was analyzed in a carbon polarimeter

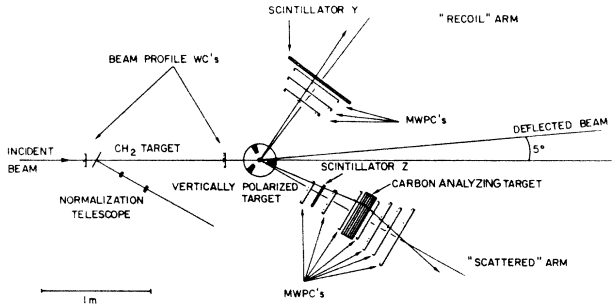

FIG. 1. Experimental setup viewed from top.

mounted directly behind the scattered proton telescope. In order to ensure a good efficiency for detecting scatterings from carbon, four chambers were used. Precise p-C effective analyzing powers (A_C) were measured with good accuracy for laboratory scattering angles between 5° and 20° and for energies from 95 to 570 MeV (Ref. 22). Each telescope was mounted on a movable platform which could be rotated about the target axis so as to allow measurement of different angular ranges. Three different arm positions corresponding to 104° c.m., 80° c.m., and 48° c.m. were used. A summary of all different conditions under which data were collected for beam and/or target and carbon scatterer conditions is summarized in Table I.

TABLE I. Beam and target configurations for data at 447, 473, 497, 517, 539, and 560 MeV as well as at 579 MeV (Ref. 17) which is mentioned for completeness. The symbol acc stands for data taken with the accelerated beam and scatt for data taken with the scattered beam. Within each condition, the beam and target polarization were frequently reversed (flipped).

Energy (MeV)	Center of angular range (deg c.m.)	Beam-polarization orientation $\hat{X}$ PPT↑↓	$\hat{Y}$ CH_2	$\hat{Y}$ $P_t \equiv 0$	$\hat{Z}$ PPT↑↓	Carbon thickness in polarimeter (cm)
447	48	acc		scatt	scatt	7
	80	scatt				7
	88	scatt		scatt	scatt	3
	104	scatt			scatt	3
473	48		scatt		scatt	7
	80	acc	scatt		scatt	7
	104	acc	scatt		acc	3
497	48	acc		scatt	acc	7
	80	scatt		scatt	scatt	7
	104	acc	scatt		acc	3
517	48	acc		acc	acc	7
	80	scatt		scatt	scatt	7
	104	acc	scatt		acc	3
539	48	acc	scatt	scatt	scatt	7
	80	scatt	scatt	scatt	scatt	7
	104	scatt	scatt	scatt	scatt	3
560	48			scatt	acc	7
	80	acc		scatt and acc	acc	7
	104		scatt	scatt		3
579	48	scatt		acc	scatt	7
	80	scatt			scatt	7
	88			scatt		7
	104	acc			scatt	3

The axes $(\hat{\mathbf{X}},\hat{\mathbf{Y}},\hat{\mathbf{Z}})$ refer to the fixed laboratory frame of the apparatus where $\hat{\mathbf{Z}}$ corresponds to the direction of the incident beam and $\hat{\mathbf{Y}}$ to the vertical downward direction. All data were taken with the PPT target, except those with the Y beam polarization orientation, for which the PPT was either unpolarized ($P_t=0$) or replaced by a CH_2 target. These last configurations allowed us to measure the polarization parameters (P,D_{n0n0}) independently of the target polarization, and were used for checking the values of the target polarization P_t. This will be discussed further on in the paper.

III. CHOICE OF OBSERVABLES

Throughout this paper we will use the scattering matrix and formalism of Ref. 23. The four-index notation X_{abcd} refers to the scattered (a), recoil (b), beam (c), and target (d) spin orientations, respectively. Each index (a, b, c, or d) can take on the values k, n, s, or 0 according to the particle polarization orientation in its attached laboratory frame. The direction $\hat{\mathbf{k}}$ is defined as being along the particle trajectory, $\hat{\mathbf{n}}$ along the normal to the scattering plane, and $\hat{\mathbf{s}}$ the orthogonal to the other two axes $(\hat{\mathbf{n}}\times\hat{\mathbf{k}})$. The 0 index stands for an unpolarized state. Where confusion can occur, indices for the scattered particle will be indicated by primes, i.e., s', n', and k'.

Prior to the start of the experiment, a study of the simplest complete set of parameters necessary for the direct reconstruction of the scattering amplitudes was made.[18,24] The observables selected are indicated in Table II. Note that each of the parameters must be measured at each given energy and angle.

Here we consider only the parameters in the bottom part of Table II. These measurements require the three possible beam polarization orientations but only a target polarization along $\hat{\mathbf{n}}$. In addition, an analysis of the two transverse components of the scattered proton polarization must be made. In this latter process, the proton scattered from the PPT target is allowed to scatter a second time from a carbon target and the polar (θ_C) and azimuthal (ϕ_C) scattering distributions observed. The azimuthal carbon scattering angle ϕ_C is defined as

$$\cos\phi_C=\hat{\mathbf{n}}\cdot\hat{\mathbf{n}}_C \quad \text{and} \quad \sin\phi_C=-\hat{\mathbf{s}}\cdot\hat{\mathbf{n}}_C\ , \tag{1}$$

where $\hat{\mathbf{n}}_C$ is the normal to the plane of the pC scattering. The observed distribution after the carbon scattering is then given by

$$\frac{d\sigma(\theta_C,\phi_C)}{d\Omega}=\sigma_C(\theta_C)[1+A_C(\theta_C)P_n\cos\phi_C - A_C(\theta_C)P_{s'}\sin\phi_C]\ . \tag{2}$$

A statistical analysis[25] of the measured distribution using Eq. (2), then yields the quantities

$$\begin{aligned}\epsilon_n(\theta_C)&=A_C(\theta_C)P_n\ ,\\ \epsilon_{s'}(\theta_C)&=-A_C(\theta_C)P_{s'}\ ,\end{aligned} \tag{3}$$

which are the two asymmetries governing the distribution. With a knowledge of A_C, the polarizations P_n and $P_{s'}$ can be fitted and determined.

Table III gives the explicit expressions for the polarizations P_n, $P_{s'}$, as a function of the double- and triple-spin parameters for the three possible incident beam orientations. Note that the number of spin-dependent parameters is reduced as compared to all possible combinations of indices due to invariance principles; therefore, $A_{00n0}=A_{000n}\equiv A$, $P_{n000}=P_{0n00}\equiv P$, and $A=P$ as well as $M_{n0nn}=P$. In fact this table is somewhat simplified as it corresponds to the experimental situation with azimuthal scattering angle $\phi=0$ (our experimental acceptance is in fact $\phi=\pm 10°$) and neglects the effect of the magnetic field surrounding the polarized target.

The effect of the magnetic field can be summarized as follows: At the carbon scatterer, only transverse-polarization components can be determined. Because of the magnetic field which precesses the proton spin, the transverse components at the carbon scatterer are not the same as at the interaction vertex in the PPT target. It has been shown[17] that the magnetic field effect can be treated as a rotation around the vertical axis $\hat{\mathbf{n}}$ by an angle ω. For this reason the horizontal transverse polarization of the scattered particle measured at the carbon analyzing target contains a mixture of the s' and k' components of the true hydrogen scattering. The polarization components measured by the polarimeter therefore correspond to the spin components of the proton along the direction $\hat{\mathbf{n}}$ and $\hat{\boldsymbol{\omega}}$ (P_n,P_ω) at the PPT where

TABLE II. Summary of data taken per energy. This paper concerns the bottom part of the table with rescattering on carbon. Moreover P is identical to A if time reversal is assumed.

Target orientation	$\hat{\mathbf{k}}$	$\hat{\mathbf{s}}$	$\hat{\mathbf{s}}$	$\hat{\mathbf{n}}$	$\hat{\mathbf{n}}$	$\hat{\mathbf{n}}$
Beam orientation	$\hat{\mathbf{k}}$	$\hat{\mathbf{k}}$	$\hat{\mathbf{s}}$	$\hat{\mathbf{s}}$	$\hat{\mathbf{n}}$	$\hat{\mathbf{k}}$
No rescattering on carbon	A_{00kk}[a]	A_{00ks}[a]	A_{00ss}[a]		A_{00nn}[b] A_{000n} A_{00n0} $(\equiv A)$	
With rescattering on carbon				D_{s0s0}[c] M_{s0sn}[c]	D_{n0n0}[c] K_{n00n}[c] $(P_{n000}\equiv P)$	D_{s0k0}[c] M_{s0kn}[c]

[a]Reference 16.
[b]Reference 15.
[c]Reference 17.

TABLE III. Relation between the polarization components of the scattered proton P_n and $P_{s'}$ and the *pp* scattering observables as analyzed on the carbon scatterer. The three possible beam orientations are considered.

		Scattered proton transverse components orientation $\hat{\mathbf{n}}$	$\hat{\mathbf{s}}'$
$\hat{\mathbf{P}}_b$	$\hat{\mathbf{n}}$	$\frac{P(1+P_bP_t)+D_{n0n0}P_b+K_{n00n}P_t}{1+P(P_b+P_t)+A_{00nn}P_bP_t}$	0
	$\hat{\mathbf{s}}$	$\frac{P+K_{n00n}P_t}{1+PP_t}$	$\frac{P_b(D_{s'0s0}+M_{s'0sn}P_t)}{1+PP_t}$
	$\hat{\mathbf{k}}$	$\frac{P+K_{n00n}P_t}{1+PP_t}$	$\frac{P_b(D_{s'0k0}+M_{s'0kn}P_t)}{1+PP_t}$

$$\hat{\omega}=\cos\omega\,\hat{\mathbf{s}}'-\sin\omega\,\hat{\mathbf{k}}'\ ,$$
$$P_\omega=\cos\omega\,P_{s'}-\sin\omega\,P_{k'}\ . \tag{4}$$

The measured observables are therefore given by

$$X_\omega\ldots=\cos\omega\,X_{s'}\ldots-\sin\omega\,X_{k'}\ldots\ , \tag{5}$$

where X is any polarization parameter. Typical values for this angle are between 7° and 13° in this energy domain.

Another important aspect of our experiment was the control over the P_t values. Referring to beam and target measurements along n as shown in Table III, one notices that D_{n0n0}, which is entirely determined by P_b and K_{n00n} entirely determined by P_t, are measured simultaneously. Using the symmetry relation

$$D_{n0n0}(\theta_{\text{c.m.}})=K_{n00n}(\pi-\theta_{\text{c.m.}}) \tag{6}$$

around 90° c.m., it is then possible to compare the target polarization with the better known value of the "scattered" beam polarization, thereby giving us a check of the P_t values independent of the NMR signal and calibration. This has turned out to be most useful, and calibration data with an unpolarized PPT or a CH_2 target were taken in order to allow this check over most of our accepted

TABLE IV. Results for the *pp* elastic-scattering parameters P, K_{n00n}, and D_{n0n0} at 560 MeV. Quoted errors are purely statistical. The beam energies quoted correspond to the reaction energies at the center of the polarized target. The estimated uncertainty is about ±3 MeV. Error on the absolute c.m. angle is 0.25°.

$\theta_{\text{c.m.}}$ (deg)	P	K_{n00n}	D_{n0n0}
34	0.598±0.022	0.268±0.067	0.831±0.062
38	0.541±0.018	0.290±0.053	0.762±0.050
42	0.528±0.017	0.397±0.049	0.727±0.047
46	0.499±0.016	0.452±0.047	0.821±0.045
50	0.475±0.015	0.433±0.046	0.808±0.043
54	0.492±0.015	0.524±0.044	0.950±0.042
58	0.391±0.014	0.450±0.043	0.739±0.041
62	0.361±0.015	0.505±0.044	0.731±0.041
66	0.341±0.009	0.579±0.027	0.772±0.028
70	0.305±0.008	0.527±0.024	0.789±0.025
74	0.240±0.008	0.532±0.024	0.789±0.024
78	0.180±0.008	0.603±0.023	0.752±0.024
82	0.128±0.008	0.618±0.023	0.749±0.023
86	0.050±0.007	0.663±0.022	0.718±0.022
90	−0.025±0.007	0.676±0.021	0.694±0.022
94	−0.065±0.008	0.674±0.023	0.638±0.023
90	0.002±0.015		0.647±0.035
94	−0.060±0.012		0.639±0.030
98	−0.111±0.012		0.640±0.029
102	−0.194±0.012		0.585±0.029
106	−0.220±0.012		0.533±0.028
110	−0.298±0.012		0.538±0.029
114	−0.331±0.013		0.520±0.031
118	−0.337±0.019		0.520±0.045

TABLE V. Same as Table IV but at 539 MeV.

$\theta_{c.m.}$ (deg)	P	K_{n00n}	D_{n0n0}
34	0.552±0.010	0.277±0.020	0.723±0.042
38	0.552±0.008	0.377±0.015	0.763±0.030
42	0.533±0.006	0.387±0.014	0.727±0.028
46	0.516±0.006	0.438±0.013	0.772±0.026
50	0.479±0.006	0.456±0.012	0.745±0.025
54	0.435±0.005	0.488±0.012	0.712±0.024
58	0.398±0.005	0.492±0.012	0.791±0.023
62	0.365±0.006	0.515±0.012	0.743±0.024
66	0.337±0.005	0.520±0.009	0.776±0.034
70	0.299±0.005	0.544±0.009	0.771±0.029
74	0.233±0.004	0.567±0.008	0.728±0.028
78	0.177±0.004	0.601±0.008	0.726±0.027
82	0.123±0.004	0.603±0.008	0.696±0.027
86	0.060±0.004	0.638±0.008	0.703±0.026
90	−0.004±0.004	0.654±0.009	0.656±0.026
94	−0.059±0.004	0.672±0.009	0.559±0.030
90	−0.014±0.005	0.639±0.011	0.653±0.024
94	−0.048±0.004	0.680±0.010	0.628±0.018
98	−0.105±0.004	0.694±0.009	0.586±0.017
102	−0.167±0.004	0.710±0.009	0.576±0.017
106	−0.219±0.004	0.728±0.010	0.532±0.017
110	−0.276±0.005	0.734±0.010	0.543±0.019
114	−0.320±0.005	0.728±0.011	0.554±0.022
118	−0.368±0.007	0.785±0.016	0.537±0.032

TABLE VI. Same as Table IV but at 517 MeV.

$\theta_{c.m.}$ (deg)	P	K_{n00n}	D_{n0n0}
34	0.544±0.015	0.259±0.026	0.771±0.024
38	0.542±0.012	0.389±0.021	0.747±0.019
42	0.520±0.011	0.390±0.019	0.765±0.017
46	0.500±0.010	0.447±0.018	0.766±0.016
50	0.471±0.010	0.437±0.017	0.761±0.015
54	0.413±0.009	0.458±0.016	0.762±0.015
58	0.384±0.009	0.485±0.016	0.742±0.015
62	0.352±0.009	0.500±0.016	0.762±0.015
66	0.316±0.005	0.535±0.010	0.729±0.027
70	0.275±0.004	0.542±0.009	0.754±0.025
74	0.221±0.004	0.548±0.009	0.772±0.024
78	0.168±0.004	0.580±0.008	0.676±0.023
82	0.111±0.004	0.580±0.008	0.641±0.023
86	0.047±0.004	0.607±0.008	0.681±0.022
90	−0.008±0.004	0.604±0.008	0.581±0.022
94	−0.070±0.005	0.637±0.008	0.644±0.024
90	0.005±0.010	0.609±0.021	0.572±0.035
94	−0.048±0.008	0.650±0.018	0.611±0.023
98	−0.094±0.007	0.651±0.018	0.578±0.023
102	−0.160±0.007	0.706±0.019	0.578±0.023
106	−0.214±0.008	0.687±0.019	0.572±0.024
110	−0.267±0.008	0.728±0.021	0.531±0.025
114	−0.313±0.009	0.768±0.024	0.528±0.029
118	−0.347±0.014	0.811±0.034	0.613±0.047

TABLE VII. Same as Table IV but at 497 MeV.

$\theta_{c.m.}$ (deg)	P	K_{n00n}	D_{n0n0}
34	0.539±0.010	0.306±0.021	0.699±0.042
38	0.530±0.007	0.350±0.016	0.784±0.031
42	0.508±0.007	0.400±0.015	0.736±0.029
46	0.487±0.006	0.438±0.014	0.711±0.027
50	0.455±0.006	0.478±0.013	0.752±0.026
54	0.415±0.006	0.529±0.013	0.745±0.024
58	0.363±0.005	0.515±0.012	0.700±0.024
62	0.335±0.005	0.537±0.012	0.708±0.025
66	0.300±0.005	0.529±0.010	0.689±0.025
70	0.265±0.005	0.546±0.009	0.691±0.023
74	0.206±0.005	0.539±0.009	0.715±0.022
78	0.178±0.004	0.570±0.008	0.671±0.021
82	0.110±0.004	0.573±0.008	0.653±0.021
86	0.053±0.004	0.592±0.008	0.666±0.020
90	0.005±0.005	0.639±0.008	0.638±0.020
94	−0.042±0.005	0.635±0.009	0.606±0.023
90	0.010±0.010	0.621±0.025	0.612±0.043
94	−0.026±0.009	0.617±0.021	0.633±0.030
98	−0.086±0.008	0.638±0.021	0.569±0.029
102	−0.157±0.008	0.665±0.022	0.611±0.029
106	−0.213±0.008	0.707±0.022	0.570±0.031
110	−0.256±0.009	0.690±0.024	0.602±0.033
114	−0.319±0.011	0.717±0.028	0.502±0.040
118	−0.345±0.017	0.664±0.041	0.611±0.075

TABLE VIII. Same as Table IV but at 473 MeV.

$\theta_{c.m.}$ (deg)	P	K_{n00n}	D_{n0n0}
34	0.540±0.013	0.309±0.025	0.710±0.052
38	0.515±0.009	0.361±0.016	0.694±0.032
42	0.499±0.008	0.421±0.015	0.703±0.027
46	0.463±0.007	0.433±0.014	0.639±0.025
50	0.429±0.006	0.470±0.013	0.686±0.023
54	0.388±0.006	0.494±0.012	0.668±0.022
58	0.363±0.006	0.529±0.012	0.670±0.022
62	0.314±0.006	0.532±0.012	0.708±0.023
66	0.291±0.005	0.527±0.011	0.681±0.025
70	0.256±0.005	0.541±0.010	0.684±0.021
74	0.198±0.005	0.548±0.009	0.690±0.021
78	0.152±0.005	0.568±0.009	0.623±0.020
82	0.103±0.004	0.565±0.009	0.635±0.020
86	0.044±0.004	0.586±0.009	0.627±0.019
90	−0.008±0.004	0.601±0.010	0.604±0.020
94	−0.060±0.005	0.595±0.011	0.595±0.027
90	0.003±0.008	0.601±0.019	0.645±0.033
94	−0.036±0.007	0.582±0.017	0.565±0.024
98	−0.093±0.007	0.627±0.017	0.571±0.024
102	−0.141±0.007	0.636±0.018	0.602±0.025
106	−0.204±0.007	0.651±0.019	0.619±0.027
110	−0.256±0.008	0.630±0.021	0.532±0.030
114	−0.314±0.010	0.684±0.026	0.545±0.037
118	−0.334±0.015	0.567±0.037	0.513±0.071

TABLE IX. Same as Table IV but at 447 MeV.

$\theta_{c.m.}$ (deg)	P	K_{n00n}	D_{n0n0}
34	0.511±0.010	0.262±0.016	0.723±0.035
38	0.501±0.008	0.334±0.011	0.639±0.024
42	0.485±0.006	0.407±0.010	0.660±0.021
46	0.471±0.006	0.443±0.009	0.708±0.020
50	0.435±0.006	0.482±0.009	0.669±0.019
54	0.396±0.005	0.492±0.008	0.682±0.018
58	0.376±0.005	0.509±0.008	0.666±0.017
62	0.328±0.005	0.492±0.009	0.666±0.018
66	0.284±0.006	0.519±0.010	
70	0.242±0.006	0.534±0.009	
74	0.203±0.005	0.553±0.009	
78	0.143±0.005	0.573±0.009	
82	0.100±0.005	0.558±0.008	
86	0.037±0.005	0.576±0.008	
90	−0.011±0.005	0.585±0.008	
94	−0.054±0.005	0.595±0.010	
74	0.204±0.008	0.558±0.018	0.655±0.020
78	0.146±0.007	0.579±0.015	0.627±0.017
82	0.108±0.007	0.558±0.015	0.616±0.016
86	0.059±0.007	0.602±0.015	0.600±0.016
90	−0.002±0.007	0.589±0.015	0.587±0.016
94	−0.066±0.007	0.600±0.015	0.571±0.016
98	−0.105±0.008	0.597±0.016	0.601±0.017
102	−0.159±0.009	0.615±0.019	0.531±0.021
90	0.012±0.007	0.607±0.014	
94	−0.037±0.007	0.597±0.012	
98	−0.076±0.007	0.621±0.012	
102	−0.146±0.007	0.619±0.013	
106	−0.176±0.007	0.632±0.013	
110	−0.244±0.008	0.668±0.015	
114	−0.300±0.010	0.670±0.019	
118	−0.339±0.015	0.612±0.028	

TABLE X. Same as Table IV (at 560 MeV) but for spin-dependent parameters $D_{\omega 0s0}$, $D_{\omega 0k0}$, $M_{\omega 0sn}$, and $M_{\omega 0kn}$. Numerical values for the mixing angle ω are given in the last column. At this energy, the mixing angle ω is somewhat different from other energy values as a similar PPT target was used, but with slightly different magnetic field.

$\theta_{c.m.}$ (deg)	$D_{\omega 0s0}$	$D_{\omega 0k0}$	$M_{\omega 0sn}$	$M_{\omega 0kn}$	ω (deg)
34		−0.065±0.055		−0.358±0.100	8.1
38		0.009±0.044		−0.334±0.079	8.2
42		0.077±0.041		−0.198±0.074	8.2
46		0.162±0.039		−0.009±0.070	8.3
50		0.258±0.037		0.004±0.067	8.4
54		0.314±0.036		0.224±0.065	8.5
58		0.368±0.034		0.029±0.063	8.5
62		0.351±0.035		0.165±0.064	8.6
66	0.688±0.024	0.360±0.024	0.110±0.075	0.257±0.044	8.7
70	0.631±0.021	0.369±0.021	−0.022±0.067	0.325±0.039	8.9
74	0.590±0.020	0.349±0.021	−0.049±0.064	0.370±0.038	9.0
78	0.627±0.020	0.342±0.020	−0.032±0.064	0.467±0.037	9.2
82	0.553±0.020	0.282±0.019	−0.129±0.063	0.445±0.036	9.3
86	0.583±0.019	0.238±0.019	−0.151±0.060	0.469±0.035	9.5
90	0.511±0.018	0.201±0.018	−0.088±0.058	0.461±0.033	9.7
94	0.480±0.019	0.124±0.019	−0.127±0.061	0.435±0.036	10.0

TABLE XI. Same as Table X but at 539 MeV.

$\theta_{c.m.}$ (deg)	$D_{\omega 0 s 0}$	$D_{\omega 0 k 0}$	$M_{\omega 0 s n}$	$M_{\omega 0 k n}$	ω (deg)
34	0.557±0.046	−0.059±0.032	0.502±0.092	−0.281±0.058	7.6
38	0.545±0.036	0.049±0.024	0.479±0.072	−0.209±0.043	7.7
42	0.609±0.033	0.108±0.022	0.571±0.067	−0.194±0.039	7.8
46	0.606±0.031	0.198±0.021	0.350±0.063	−0.091±0.037	7.8
50	0.583±0.030	0.255±0.020	0.423±0.060	0.007±0.035	7.9
54	0.632±0.028	0.344±0.019	0.322±0.057	0.102±0.034	8.0
58	0.547±0.027	0.330±0.018	0.198±0.056	0.176±0.032	8.1
62	0.586±0.028	0.379±0.018	0.177±0.058	0.214±0.033	8.2
66	0.573±0.017	0.364±0.017	0.109±0.032	0.271±0.031	8.3
70	0.582±0.016	0.361±0.016	0.126±0.030	0.285±0.029	8.4
74	0.564±0.015	0.386±0.015	0.103±0.029	0.347±0.028	8.5
78	0.535±0.015	0.326±0.015	0.025±0.028	0.372±0.027	8.6
82	0.534±0.015	0.282±0.015	−0.053±0.027	0.349±0.026	8.8
86	0.502±0.014	0.241±0.014	−0.101±0.026	0.363±0.026	9.0
90	0.453±0.014	0.250±0.014	−0.119±0.026	0.308±0.025	9.2
94	0.488±0.016	0.141±0.016	−0.119±0.031	0.362±0.029	9.4
90	0.503±0.018	0.214±0.017	−0.063±0.037	0.367±0.035	9.2
94	0.477±0.016	0.172±0.015	−0.160±0.033	0.438±0.031	9.4
98	0.440±0.016	0.132±0.015	−0.102±0.032	0.340±0.031	9.7
102	0.411±0.016	0.071±0.015	−0.158±0.032	0.329±0.031	10.0
106	0.413±0.016	0.014±0.016	−0.085±0.033	0.407±0.032	10.4
110	0.410±0.017	−0.020±0.016	−0.173±0.035	0.289±0.034	10.8
114	0.359±0.019	−0.102±0.019	−0.183±0.040	0.234±0.038	11.2
118	0.352±0.028	−0.151±0.026	−0.182±0.058	0.207±0.055	11.8

TABLE XII. Same as Table X but at 517 MeV.

$\theta_{c.m.}$ (deg)	$D_{\omega 0 s 0}$	$D_{\omega 0 k 0}$	$M_{\omega 0 s n}$	$M_{\omega 0 k n}$	ω (deg)
34	0.462±0.033	−0.066±0.027	0.554±0.064	−0.449±0.051	7.8
38	0.557±0.026	−0.007±0.021	0.565±0.050	−0.237±0.040	7.8
42	0.540±0.023	0.071±0.019	0.435±0.045	−0.152±0.037	7.9
46	0.570±0.022	0.137±0.018	0.432±0.043	−0.175±0.035	7.9
50	0.596±0.020	0.207±0.017	0.451±0.040	−0.059±0.033	8.0
54	0.602±0.019	0.266±0.017	0.319±0.038	0.055±0.032	8.1
58	0.607±0.019	0.321±0.016	0.262±0.037	0.095±0.031	8.2
62	0.614±0.019	0.332±0.016	0.230±0.038	0.163±0.031	8.3
66	0.592±0.018	0.344±0.017	0.114±0.034	0.199±0.034	8.4
70	0.596±0.016	0.353±0.016	0.108±0.031	0.220±0.030	8.5
74	0.568±0.015	0.344±0.015	0.053±0.030	0.325±0.029	8.6
78	0.582±0.015	0.323±0.015	0.021±0.029	0.324±0.028	8.7
82	0.550±0.015	0.275±0.015	−0.048±0.028	0.346±0.028	8.9
86	0.527±0.014	0.253±0.014	−0.045±0.028	0.341±0.027	9.1
90	0.479±0.014	0.212±0.014	−0.145±0.027	0.362±0.027	9.3
94	0.541±0.015	0.144±0.016	−0.097±0.031	0.325±0.030	9.6
90	0.534±0.020	0.247±0.017	−0.083±0.043	0.430±0.035	9.3
94	0.516±0.017	0.216±0.015	−0.111±0.038	0.463±0.031	9.6
98	0.520±0.017	0.132±0.015	−0.252±0.038	0.378±0.031	9.9
102	0.492±0.017	0.079±0.015	−0.096±0.038	0.449±0.031	10.2
106	0.475±0.018	0.022±0.016	−0.151±0.040	0.406±0.032	10.5
110	0.504±0.019	0.007±0.016	−0.159±0.043	0.342±0.034	11.0
114	0.434±0.022	−0.080±0.019	−0.108±0.049	0.357±0.040	11.4
118	0.415±0.031	−0.086±0.027	−0.179±0.069	0.290±0.056	12.0

TABLE XIII. Same as Table X but at 497 MeV.

$\theta_{c.m.}$ (deg)	$D_{\omega 0s0}$	$D_{\omega 0k0}$	$M_{\omega 0sn}$	$M_{\omega 0kn}$	ω (deg)
34	0.406±0.035	−0.044±0.044	0.397±0.067	−0.243±0.090	7.8
38	0.424±0.026	0.125±0.032	0.425±0.050	−0.167±0.067	7.9
42	0.480±0.024	0.077±0.030	0.440±0.046	−0.146±0.061	7.9
46	0.495±0.022	0.170±0.028	0.376±0.043	−0.171±0.057	8.0
50	0.525±0.021	0.239±0.026	0.288±0.041	−0.057±0.054	8.1
54	0.516±0.020	0.265±0.025	0.251±0.039	0.067±0.052	8.2
58	0.554±0.019	0.261±0.024	0.240±0.038	0.056±0.050	8.2
62	0.601±0.020	0.304±0.025	0.162±0.039	0.165±0.051	8.3
66	0.583±0.026	0.327±0.017	0.177±0.043	0.168±0.031	8.4
70	0.604±0.023	0.346±0.015	0.076±0.038	0.269±0.026	8.6
74	0.558±0.022	0.349±0.015	0.074±0.037	0.277±0.025	8.7
78	0.577±0.021	0.294±0.015	0.050±0.036	0.307±0.024	8.9
82	0.597±0.021	0.283±0.015	−0.018±0.035	0.312±0.024	9.1
86	0.564±0.020	0.247±0.014	−0.031±0.034	0.348±0.023	9.3
90	0.549±0.020	0.215±0.014	−0.128±0.034	0.360±0.023	9.5
94	0.547±0.023	0.193±0.016	−0.114±0.039	0.393±0.027	9.7
90	0.542±0.022	0.228±0.022	−0.063±0.045	0.360±0.044	9.5
94	0.529±0.019	0.179±0.018	−0.139±0.039	0.385±0.037	9.7
98	0.569±0.019	0.130±0.018	−0.193±0.038	0.358±0.037	10.0
102	0.483±0.019	0.073±0.018	−0.215±0.039	0.379±0.038	10.3
106	0.515±0.020	0.070±0.019	−0.206±0.041	0.435±0.039	10.7
110	0.493±0.021	−0.029±0.021	−0.162±0.044	0.330±0.042	11.1
114	0.518±0.025	−0.085±0.024	−0.234±0.052	0.352±0.049	11.6
118	0.468±0.035	−0.062±0.034	−0.239±0.074	0.293±0.071	12.2

TABLE XIV. Same as Table X but at 473 MeV.

$\theta_{c.m.}$ (deg)	$D_{\omega 0s0}$	$D_{\omega 0k0}$	$M_{\omega 0sn}$	$M_{\omega 0kn}$	ω (deg)
34		−0.122±0.034		−0.397±0.061	7.9
38		0.011±0.024		−0.278±0.043	8.0
42		0.050±0.020		−0.188±0.037	8.0
46		0.097±0.019		−0.165±0.034	8.1
50		0.183±0.018		−0.007±0.032	8.2
54		0.239±0.017		0.046±0.031	8.3
58		0.257±0.017		0.065±0.030	8.4
62		0.313±0.018		0.134±0.030	8.5
66	0.615±0.017	0.302±0.017	0.207±0.030	0.153±0.031	8.6
70	0.616±0.014	0.315±0.016	0.119±0.027	0.226±0.026	8.7
74	0.621±0.013	0.292±0.015	0.106±0.026	0.205±0.025	8.9
78	0.586±0.013	0.326±0.015	0.057±0.026	0.314±0.025	9.0
82	0.586±0.013	0.283±0.015	−0.003±0.025	0.335±0.024	9.2
86	0.597±0.012	0.254±0.014	−0.027±0.024	0.346±0.024	9.4
90	0.578±0.012	0.192±0.014	−0.076±0.024	0.328±0.024	9.7
94	0.586±0.015	0.147±0.016	−0.074±0.029	0.337±0.029	9.9
90	0.578±0.018	0.238±0.017	−0.103±0.034	0.362±0.035	9.7
94	0.566±0.016	0.207±0.015	−0.144±0.030	0.371±0.031	9.9
98	0.569±0.016	0.133±0.015	−0.121±0.030	0.362±0.031	10.2
102	0.547±0.016	0.108±0.015	−0.153±0.032	0.379±0.031	10.5
106	0.538±0.017	0.032±0.016	−0.191±0.034	0.412±0.034	11.0
110	0.525±0.018	0.001±0.018	−0.234±0.038	0.314±0.037	11.4
114	0.510±0.022	−0.069±0.022	−0.186±0.046	0.289±0.046	11.9
118	0.434±0.031	−0.088±0.031	−0.215±0.065	0.379±0.064	12.5

range of angular measurements ($\theta_{\text{c.m.}}=34°-118°$) as indicated in Table I. In general a good agreement was observed for the P_t values. On a small fraction of the data, a normalization factor was found necessary, this mainly after a rotation of the target coil orientations while changing from 80° to 140° positions (namely, 8% for the 104° X and Z positions at 447 MeV and 6% for the 80° X at 473 MeV). Unfortunately no recalibration of the target polarization had been performed after these changes.

IV. ANALYSIS

To obtain the asymmetries ϵ_n and ϵ_ω along the n and ω axes, a Fourier analysis of the measured carbon-scattering distribution was performed.[25] The polarization components P_n, P_ω, could then be found by dividing the ϵ's by the analyzing power A_C. These pC analyzing powers[22] were determined from a two-dimensional empirical formula fitting our previously measured data points as well as some TRIUMF data for the same carbon-scatterer thickness (3 cm). Reasonable agreement with other available data have been found except for a small discrepancy above 200 MeV where the 6-cm TRIUMF data are higher by 4%. The polarization parameters P_{n000}, D_{n0n0}, K_{n00n}, $D_{\omega0k0}$, $D_{\omega0s0}$, $M_{\omega0sn}$, and $M_{\omega0kn}$, were extracted by fitting expressions of the type given in Table III, which relate the measured polarization to the spin observables. The finite azimuthal acceptance and magnetic-field effects were also taken into account. This complicates the expressions in Table III somewhat; for instance, with P_b along $\hat{\mathbf{n}}$, the polarization along $\hat{\mathbf{n}}$ becomes

$$\frac{P(1+P_bP_t\cos^2\phi)+D_{n0n0}P_b\cos\phi+K_{n00n}P_t\cos\phi+M_{n0ss}P_bP_t\sin^2\phi}{1+P(P_b+P_t)\cos\phi+A_{00nn}P_tP_b\cos^2\phi+A_{00ss}P_bP_t\sin^2\phi}\ . \tag{7}$$

A full description of the analysis used can be found in Ref. 17. Since the parameters in the denominators have already been measured,[15,16] smooth values from a fit by the Saclay-Geneva phase-shift analysis were used, and only the dominant parameters with $\cos\phi$, $\cos^2\phi$ in the numerator fitted. The residual terms in $\sin^2\phi$, i.e., M_{n0ss}, M_{s0sn}, and M_{k0ns}, which contribute very little (maximum value $\sin^2\phi=0.03$) were not fitted. Values were taken from phase-shift predictions instead.

Systematic effects in these data can be divided into two categories: the first is due to the uncertainty in the energy at the carbon scattering, while the second is due to nonsymmetric absorption in the polarimeter. Both have been evaluated and corrected. A precise knowledge of the energy at which the carbon scattering takes place is particularly important for low-energy protons (below 200 MeV) as in this region the carbon analyzing power varies rapidly with energy ($\Delta A_C/A_C=5\%$ for a 5-MeV change in kinetic energy). To know the correct scattering energy, we must (a) know the exact beam energy, (b) know the hor-

TABLE XV. Same as Table X but at 447 MeV.

$\theta_{\text{c.m.}}$ (deg)	$D_{\omega0s0}$	$D_{\omega0k0}$	$M_{\omega0sn}$	$M_{\omega0kn}$	ω (deg)
34	0.295±0.032	−0.200±0.032	0.511±0.060	−0.320±0.049	8.0
38	0.344±0.022	−0.043±0.022	0.421±0.042	−0.231±0.035	8.1
42	0.385±0.020	0.009±0.020	0.402±0.038	−0.196±0.031	8.2
46	0.466±0.018	0.090±0.018	0.398±0.035	−0.134±0.029	8.3
50	0.497±0.017	0.153±0.017	0.380±0.033	−0.071±0.027	8.3
54	0.518±0.016	0.231±0.016	0.291±0.031	0.044±0.025	8.4
58	0.553±0.016	0.266±0.016	0.288±0.030	0.033±0.024	8.5
62	0.615±0.016	0.258±0.019	0.274±0.030	0.071±0.031	8.6
66	0.549±0.020	0.307±0.019	0.146±0.038	0.172±0.033	8.7
70	0.614±0.018	0.341±0.017	0.127±0.034	0.186±0.029	8.9
74	0.579±0.017	0.315±0.016	0.030±0.032	0.261±0.028	9.0
78	0.572±0.017	0.280±0.016	0.013±0.031	0.260±0.028	9.2
82	0.614±0.016	0.263±0.016	0.004±0.031	0.274±0.027	9.4
86	0.571±0.016	0.278±0.015	−0.033±0.031	0.246±0.027	9.6
90	0.590±0.016	0.219±0.015	0.001±0.030	0.273±0.027	9.9
94	0.555±0.019	0.163±0.018	−0.082±0.035	0.311±0.031	10.1
90	0.578±0.026	0.179±0.024	−0.051±0.051	0.235±0.045	9.9
94	0.562±0.023	0.206±0.021	−0.047±0.044	0.306±0.039	10.1
98	0.541±0.023	0.137±0.021	−0.043±0.043	0.356±0.039	10.4
102	0.537±0.024	0.089±0.022	−0.123±0.045	0.273±0.041	10.8
106	0.528±0.025	0.054±0.023	−0.203±0.049	0.334±0.044	11.2
110	0.573±0.029	−0.002±0.026	−0.146±0.055	0.305±0.049	11.7
114	0.441±0.035	−0.019±0.032	−0.061±0.068	0.298±0.060	12.1
118	0.395±0.051	−0.095±0.048	−0.269±0.100	0.398±0.090	12.8

izontal position of the beam in the PPT target since the energy loss in the target by the scattered particle depends on the horizontal vertex position X_v, (c) monitor the instability in X_v vertex position between measurements with P_b +,− and P_t +,−, (d) calculate the difference between energy loss for central position and mean energy loss, and (e) take into account the fact that the external bins in θ_H are not uniformly populated due to acceptance dropoff. A calculation shows that these effects are negligible for kinetic energy above 200 MeV. Below this point the most significant correction is for $\theta_{c.m.}=118°$ (corresponding for the 447-MeV data to 109-MeV proton incident on the carbon) where a total correction of 2.7% on the parameters is necessary. In the second category, one

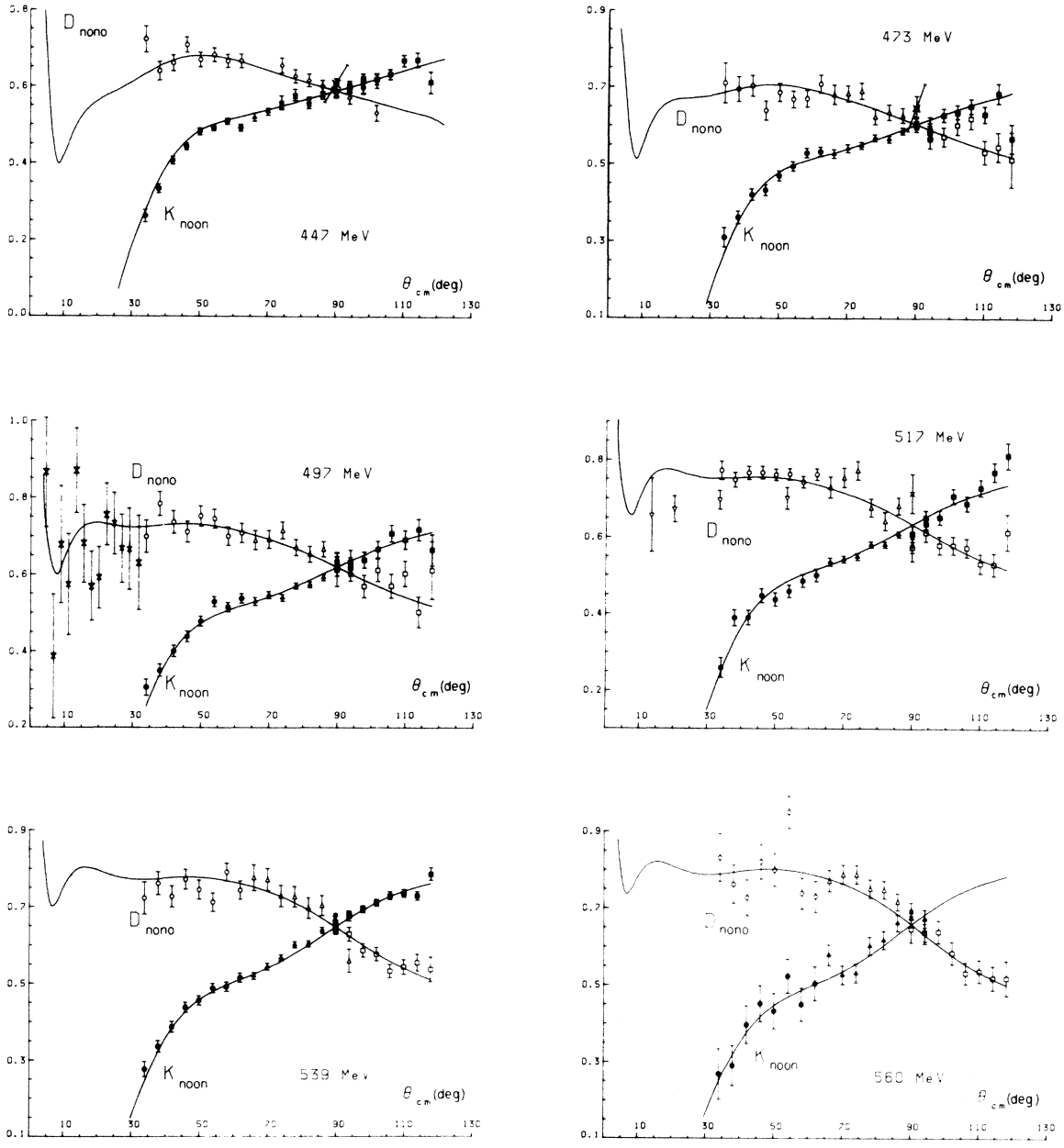

FIG. 2. D_{n0n0},K_{n00n} for *pp* elastic at 447, 473, 497, 517, 539, and 560 MeV as a function of the c.m. scattering angle. The three different symbols (dots, triangles, squares) correspond to the three different turn-table settings used to cover the whole angular range. The solid curve is Saclay-Geneva phase-shift-analysis fit using these data and our previous CERN SC and SIN data. The small-angle data at 497 MeV are our SIN data (Ref. 28), the 90° data points are from LAMPF (Ref. 27) and finally the 517-MeV D_{n0n0} data are from TRIUMF (Ref. 26).

must take into account the following effects: (1) the particles incident on the carbon analyzer do not all arrive perpendicularly to the normal, (2) after the carbon scattering, the particles scattered to the outside of the polarimeter go through more thicknesses of carbon and chamber material than those scattered along the center axis. They have therefore a higher probability of being absorbed or rescattered. These effects could result in an artificial asymmetry depending on the incident angle. It turns out that these second category effects are largest for P_{n000}, and somewhat less for D_{n0n0},K_{n00n} because of the beam and target flipping. Like the first category effect, the second category effects are also largest around 118° c.m. where A_C is small. Sizable effects also appear at the lower extreme of our angular range ($\Delta P = 0.005$) where 7-cm carbon is used.

Other systematic effects include normalization errors due to uncertainties on the beam and target polarizations and carbon analyzing power A_C. These have been studied and can be summarized as follows: 2—3 % on P, 6—7 % on K_{n00n}, 1—2 % on D, 6% on M. For data taken with the "accelerated" beam, however, the polarization is less well known, so that the two last values become 3—4 % on D and 7—8 % on M. Note that these errors are not independent (for details see Tables IV and V of Ref. 17).

V. RESULTS AND CONCLUSIONS

The experimental results are given in Tables IV—XV along with their statistical errors, for each energy, respectively. The mixing angle ω for each $\theta_{\text{c.m.}}$ bin is also quot-

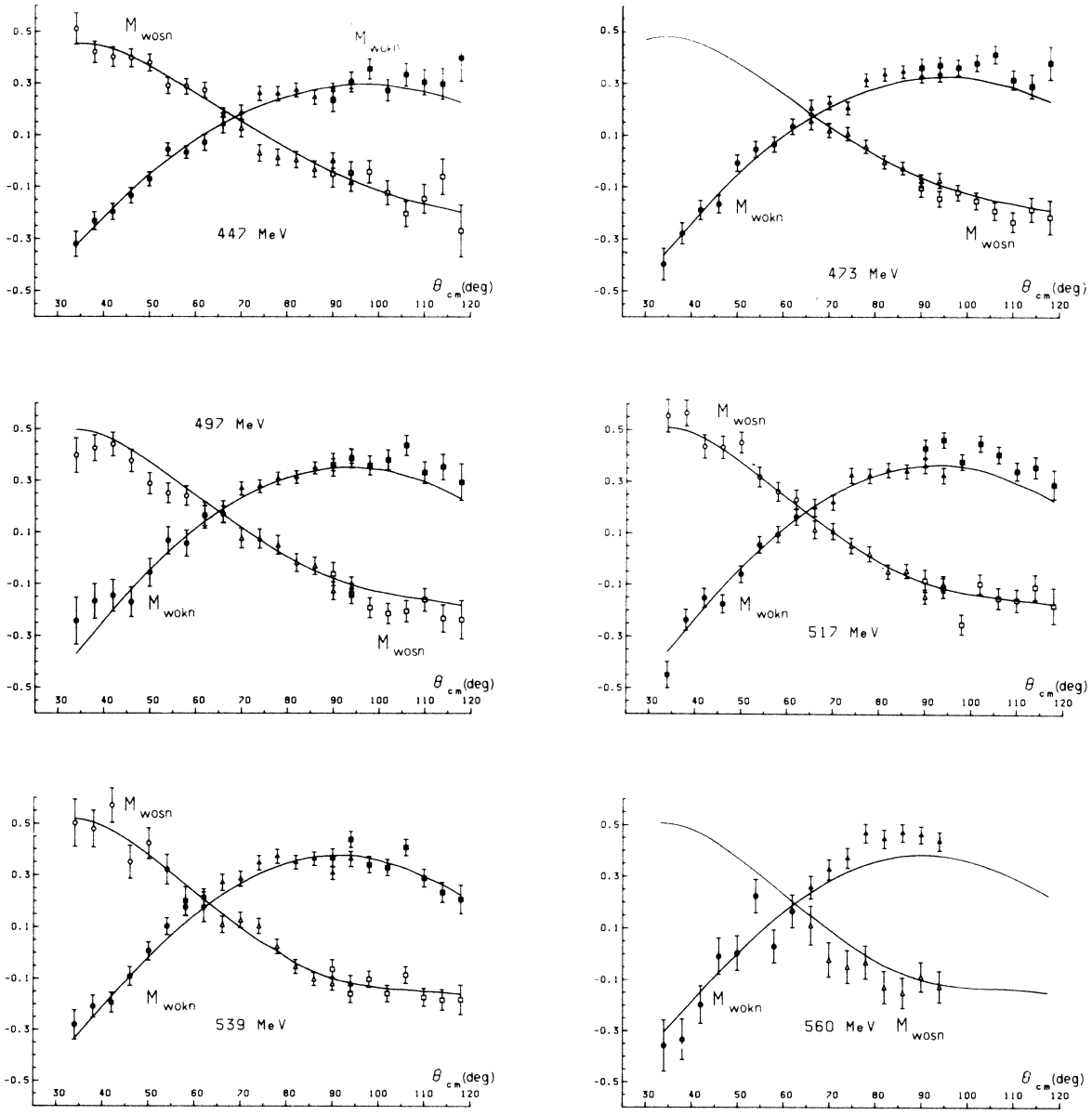

FIG. 3. $M_{\omega 0sn}$,$M_{\omega 0kn}$ for pp elastic scattering as a function of the c.m. scattering angle.

ed. In Figs. 2 and 3 are plotted the results for D_{n0n0},K_{n00n} and $M_{\omega 0sn}$,$M_{\omega 0kn}$, respectively, along with other available data. Figure 4 shows the D_{s0s0} ($\equiv R$) and D_{s0k0} ($\equiv A$) parameters themselves, using Eq. (5) in which the values for D_{k0s0} ($\equiv R'$) and D_{k0k0} ($\equiv A'$) parameters were taken from phase-shift analysis. A discrepancy is seen with the 517-MeV TRIUMF data.[26] The LAMPF data, on the other hand, were in good agreement in the overlapping energy region.[27] One observes a smooth continuation towards small angles as measured at SIN.[28] The solid lines on the figures are results from an energy-dependent PSA analysis using as a data base only our previous data from CERN SC (Refs. 29 and 30) and SIN (Refs. 15–17 and 28) and the present data. The only external data are elastic $d\sigma/d\Omega$ and total inelastic cross section.[31] A good fit to the data ($\chi^2/\nu \approx 1.33$) was obtained with the same energy dependence as was used before.

The triple-spin parameters are large at all six energies and vary widely within the observed angular range. It is most surprising to notice that the shape and magnitude of all these parameters vary little with energy from 447 to 579 MeV. The same features are observed throughout, i.e., a large magnitude for the two- and three-spin parame-

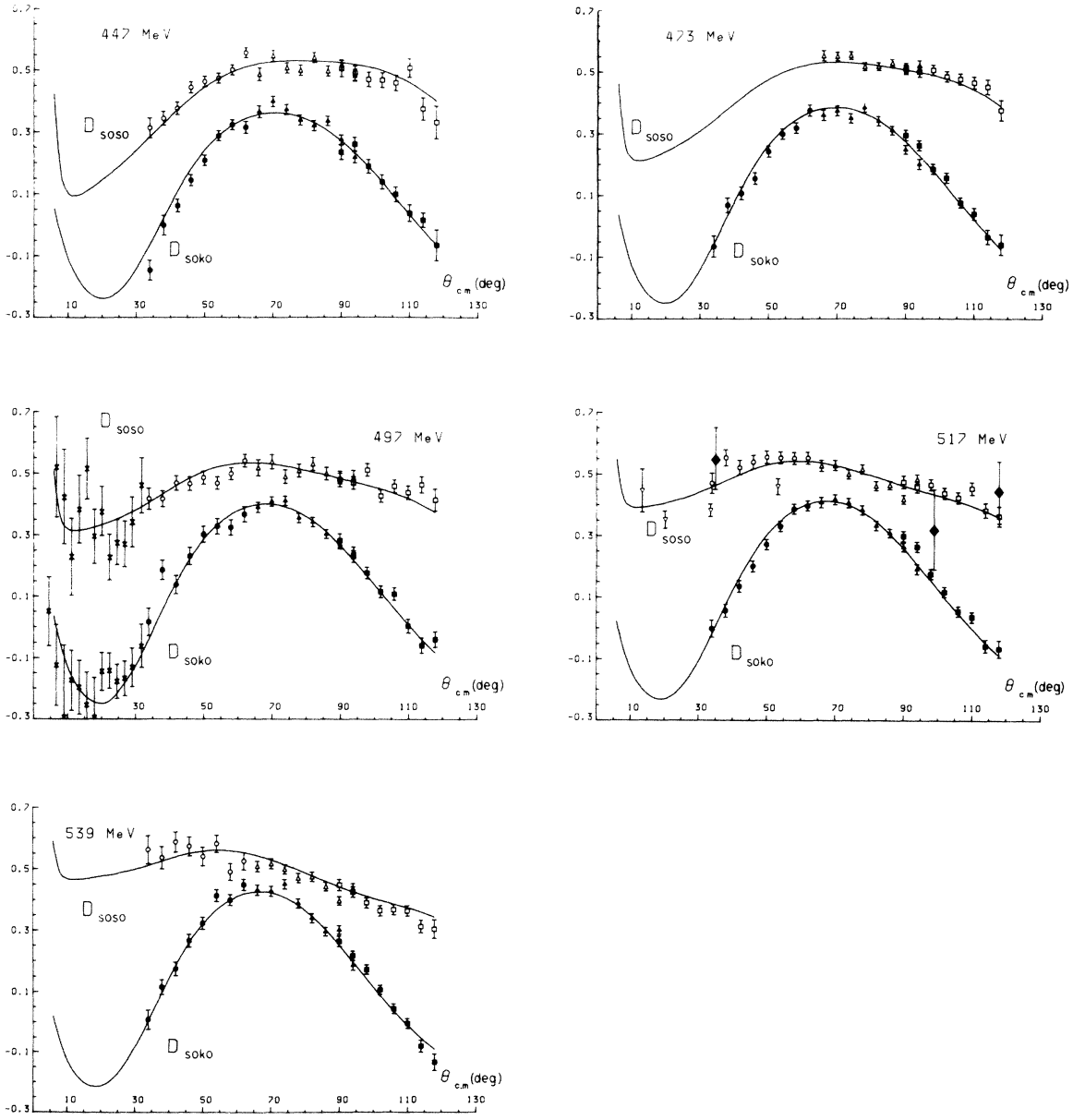

FIG. 4. D_{s0s0} ($\equiv R$), D_{s0k0} ($\equiv A$) for *pp* elastic scattering as a function of the c.m. scattering angle. At 517 MeV the small-angle D_{s0s0} data (shown as inverted triangles) are from TRIUMF (Ref. 26), the larger-angle ones (shown as a ♦) are from Ref. 31. As the 560-MeV data cover a smaller angular range, no attempt to recalculate the R and A parameters was done.

ters, along with a smooth angular variation. This last point is in contrast with the πd elastic channel where strong oscillations are reported.

The 560-MeV data are of particular interest as this incident kinetic energy in the pp system corresponds to 134 MeV in the πd elastic scattering where t_{20} was observed to have a pronounced and rapid angular oscillatory behavior.[3] Nearby π incident energies show no oscillatory structure. At this energy (560 MeV) unfortunately a pp amplitude reconstruction could not be performed as our experimental data set was not sufficient. From the energy behavior derived from nearby data, one could see that no violent change was observed at this very energy in pp elastic scattering. Data can be fitted with smooth energy-dependent functions. This indicates that the 560-MeV data show no surprising behavior, neither in magnitude or in angular dependence.

We have shown that such an experimental program on polarization measurements is feasible today within reasonable time limits, thanks mainly to the large availability of the high intensity proton beam at SIN. We have also shown that measurements of 3-spin parameters with good precision are feasible. A logical continuation of this type of experimental program could be done at the kaon factories.

ACKNOWLEDGMENTS

We would like to thank the Swiss Institute for Nuclear Research for its invaluable technical assistance during the experiment and express our special gratitude to Professor J. P. Blaser, its director. During the course of this program, support from Professor W. Baumgartner, Professor J. Deutsch, Professor H. J. Gerber, Professor R. Mermod as well as Dr. M. Daum and Dr. F. Lehar were greatly appreciated. We would also like to thank the technical staff of the University of Geneva, in particular the electronic (Mr. Richeux) and mechanical workshops (Mr. Perrin). This work was supported by the Swiss National Science Foundation and the Convention Intercantonale d'Enseignement du 3eme cycle de la Physique en Suisse Romande. We would like to thank our funding agencies and SIN for supporting this laborious and long research program.

---

*Present address: Physics Department, Harvard University, Cambridge, MA 02138.

†Present address: Institut de Génie Atomique, Department of Physics, Ecole Polytechnique Fédérale de Lausanne, 1015 Lausanne, Switzerland.

[1]I. P. Auer, E. Colton, H. Halpern, D. Hill, H. Spinka, G. Theodosiou, D. Underwood, Y. Watanabe, and A. Yokosawa, Phys. Lett. **67B**, 113 (1978).

[2]G. R. Smith, E. L. Mathie, E. T. Boschitz, C. R. Ottermann, S. Mango, J. A. Konter, M. Daum, M. Meyer, R. Olszewski, and F. Vogler, Phys. Rev. C **29**, 2206 (1984).

[3]W. Gruebler, J. Ulricht, V. Koenig, P. A. Schmetzbach, K. Elsener, D. Schweizer, M. Merdzanaud, and A. Chrisholm, Phys. Rev. Lett. **49**, 444 (1982); V. Koenig, A. Chrisholm, W. Gruebler, J. Ulbricht, P. A. Schmetzbach, M. Merdzan, and K. Elsener, J. Phys. G **9**, L211 (1983).

[4]R. J. Holt, J. R. Specht, E. J. Stephenson, B. Zeidman, R. L. Burman, J. S. Frank, M. J. Leitch, J. D. Moses, M. A. Yates-William, R. M. Lszewski, and R. P. Redwine, Phys. Rev. Lett. **43**, 1229 (1979); R. J. Holt, J. R. Specht, K. Stephenson, B. Zeidman, J. S. Frank, M. J. Leitch, J. D. Moses, E. J. Stephenson, and R. M. Laszewski, *ibid.* **47**, 472 (1981); E. Ungricht, W. S. Freeman, D. F. Geesaman, R. J. Holt, J. R. Specht, B. Zeidman, E. J. Stephenson, J. D. Moses, M. Farkhondeh, S. Gilad, and R. P. Redwine, *ibid.* **52**, 333 (1984).

[5]Y. M. Shin, K. Itoh, N. R. Stevenson, D. R. Gill, D. F. Ottewall, G. G. Wait, T. E. Drake, D. F. Frekersa, R. B. Schubank, and G. J. Lolos, Phys. Rev. Lett. **55**, 2672 (1985).

[6]E. Boschitz (private communication).

[7]H. Garcilazo, Phys. Rev. Lett. **53**, 652 (1984); M. P. Locher *et al.*, Adv. Nucl. Phys. (to be published).

[8]N. Hoshizaki, Prog. Theor. Phys. **61**, 129 (1979).

[9]R. A. Arndt, L. D. Roper, R. A. Bryan, R. B. Clark, B. J. VerWest, and P. Signell, Phys. Rev. D **28**, 97 (1983).

[10]J. Bystricky, C. Lechanoine-Leluc, and F. Lehar, Saclay Report No. 82-12, 1982 (unpublished).

[11]R. Dubois, D. Axen, R. Keeler, M. Comyn, D. G. A. Ludgate, J. R. Richardson, N. M. Stewart, A. S. Clough, and D. V. Bugg, Nucl. Phys. **A377**, 544 (1982).

[12]W. M. Kloet and J. A. Tjon, Phys. Lett. **106B**, 24 (1981).

[13]F. Lehar, contribution to the 6th International Symposium on Polarization Phenomena in Nuclear Physics, Osaka, 1985 [J. Phys. Soc. Jpn. Suppl. **55**, 284 (1986)].

[14]L. Puzikov, R. Ryndin, and J. Smorodinsky, Nucl. Phys. **3**, 436 (1957).

[15]D. Besset, Q. H. Do, B. Favier, R. Hausammann, E. Heer, R. Hess, C. Lechanoine, W. R. Leo, D. Rapin, D. W. Werren, Ch. Weddigen, J. M. Cameron, S. Jaccard, and S. Mango, Nucl. Phys. **A345**, 435 (1980).

[16]E. Aprile, R. Hausammann, E. Heer, R. Hess, C. Lechanoine-Leluc, W. R. Leo, S. Morenzoni, Y. Onel, D. Rapin, and S. Mango, Phys. Rev. D **28**, 21 (1983).

[17]E. Aprile, R. Hausammann, E. Heer, R. Hess, C. Lechanoine-Leluc, W. R. Leo, S. Morenzoni, Y. Onel, D. Rapin, and S. Mango, Phys. Rev. D **27**, 2600 (1983).

[18]R. Hausammann, Ph.D. thesis, University of Geneva, 1982.

[19]E. Aprile, C. Eiseneggar, R. Hausammann, E. Heer, R. Hess, C. Lechanoine-Leluc, W. R. Leo, S. Morenzoni, Y. Onel, and D. Rapin, Phys. Rev. Lett. **46**, 1047 (1981).

[20]E. Aprile, R. Hausammann, E. Heer, R. Hess, C. Lechanoine-Leluc, W. R. Leo, S. Morenzoni, Y. Onel, and D. Rapin, Phys. Rev. Lett. **47**, 1360 (1981).

[21]D. Besset, Q. H. Do, B. Favier, L. G. Greeniaus, E. Heer, R. Hess, C. Lechanoine-Leluc, D. Rapin, D. W. Werren, M. Daum, S. Mango, E. Steiner, G. Vecsey, and Ch. Weddigen, Nucl. Instrum. Methods **184**, 365 (1981).

[22]E. Aprile-Giboni, R. Hausammann, E. Heer, R. Hess, C. Lechanoine-Leluc, W. R. Leo, S. Morenzoni, Y. Onel, and D. Rapin, Nucl. Instrum. Methods **215**, 147 (1983).

[23]J. Bystricky, F. Lehar, and P. Winternitz, J. Phys. (Paris) **39**, 1 (1978).

[24]D. Besset, B. Favier, L. G. Greeniaus, R. Hess, D. Rapin, D. W. Werren, and C. Weddigen, Nucl. Instrum. Methods **148**, 129 (1978).

[25]D. Besset, B. Favier, L. G. Greeniaus, R. Hess, C. Lechanoine, D. Rapin, and D. W. Werren, Nucl. Instrum. Methods **166**, 515 (1979).

[26]D. V. Bugg, J. A. Edgington, C. Amsler, R. C. Brown, C. J. Oram, K. Shakarchi, N. W. Stewart, G. A. Ludgate, A. S. Clough, D. Axen, S. Jaccard, and J. Vavra, J. Phys. G **4**, 1025 (1978).

[27]C. Hollas, D. J. Cremans, R. D. Ransome, P. J. Riley, B. E. Bonner, M. W. McNaughton, and S. Wood, Phys. Lett. **143B**, 343 (1984).

[28]D. Besset, Q. H. Do, B. Favier, L. G. Greeniaus, R. Hess, C. Lechanoine, D. Rapin, D. W. Werren, and Ch. Weddigen, Phys. Rev. D **21**, 580 (1980).

[29]D. Aebischer, B. Favier, L. G. Greeniaus, R. Hess, A. Junod, C. Lechanoine, J. C. Nickles, D. Rapin, C. Richard-Serre, and D. W. Werren, Phys. Rev. D **13**, 2478 (1976).

[30]D. Aebischer, B. Favier, L. G. Greeniaus, R. Hess, A. Junod, C. Lechanoine, J. C. Nickles, D. Rapin, and D. W. Werren, Nucl. Phys. **A276**, 445 (1977).

[31]J. Bystricky and F. Lehar, *Nucleon-Nucleon Scattering Data,* edited by H. Behrens and G. Ebel (Physics Data Nos. 11-1, 11-2, and 11-3) (Fachinformationszentrum, Karlsruhe, 1978 and 1981).